

Coherent network analysis for triggered gravitational wave burst searches

K Hayama¹, S D Mohanty¹, M Rakhmanov², S Desai²

¹The University of Texas at Brownsville, 80 Fort Brown, Brownsville, Texas, 78520, USA.

² Department of Physics, Pennsylvania State University, University Park, PA 16802, USA.

E-mail: kazu@phys.utb.edu

Abstract. Searches for gravitational wave bursts that are triggered by the observation of astronomical events require a different mode of analysis than all-sky, blind searches. For one, much more prior information is usually available in a triggered search which can and should be used in the analysis. Second, since the data volume is usually small in a triggered search, it is also possible to use computationally more expensive algorithms for tasks such as data pre-processing that can consume significant computing resources in a high data-volume un-triggered search. From the statistical point of view, the reduction in the parameter space search volume leads to higher sensitivity than an un-triggered search. We describe here a data analysis pipeline for triggered searches, called **RIDGE**, and present preliminary results for simulated noise and signals.

1. Introduction

Gravitational wave (GW) searches that are triggered by the observation of an astronomical event have some aspects that are fundamentally different from all-sky or un-triggered searches. First of all, the non-GW observations furnish a wealth of prior information that can guide the GW data analysis. For instance, in the case of a Gamma-ray Burst (GRB) trigger, we usually know the sky location and, sometimes, the distance to the source. Based on the type of GRB, long-soft or short-hard, one can look for qualitatively different signals: short duration bursts for the former and binary inspiral signals for the latter. Second, there are many data pre-processing algorithms available in the literature that have been demonstrated to be useful but have not been used in untriggered searches because of a natural selection effect: finite computational resources pick the computationally least expensive algorithm. Triggered searches, on the other hand, usually involve much smaller data volumes and, consequently, allow us the freedom to experiment with algorithms.

In this paper, we describe results from one such ongoing experiment of using new algorithms for analyzing data from the LIGO, GEO and Virgo detectors for triggered searches. We use new algorithms for both the data pre-processing (*conditioning*) and the search part of the analysis pipeline. The code for the pipeline, called **RIDGE**, is written mostly in matlab. We will not describe the code in any detail in this paper but focus on the algorithms and results.

2. Data analysis components

A typical triggered search involves several components [1]. First, a mechanism is required to collect trigger information. This is already well developed and nearly automated within the LIGO Scientific Collaboration (LSC), at least as far as GCN [2] triggers are concerned. Second, given the wealth of astrophysical prior information associated with most triggers, we need proper mathematical tools to incorporate this information into our analysis. So far, this aspect of a triggered search has seen only limited advances. The most detailed use of prior information has been in the search [3] for GWs from the SGR-1806-20 event [4] where X-ray intensity oscillations associated with the flare were used to motivate a search for quasi-monochromatic signals at specific frequencies. However, more work is needed in this area, especially on the use of Bayesian approaches modeled after the ones used for a different type of “triggered” search [5], namely GWs from known pulsars in the Galaxy. The other components required in a typical triggered search, as in any other search, are *data conditioning* and the generation of a detection statistic.

2.1. Data conditioning in RIDGE

The purpose of data conditioning is to mitigate the effect of known instrumental artifacts in the data. In *RIDGE* this is done in a two step process. First, the *noise floor* of the power spectral density (PSD) of noise is estimated using a running median [6]. Fig. 1 shows the PSD of 2 sec of simulated detector noise with a power spectral density approximating the LIGO SRD curve for the 4km detectors. Superimposed on the estimated PSD is the running median estimate of the noise floor. The main advantage of the running median is its ability to reject outliers. In this particular case, the outliers are the narrowband noise artifacts arising from sources such as power line interference (modeled as sinusoids in this particular example).

If $S(f)$ denotes the running median estimate of the PSD, a digital filter with a transfer function $T(f)$ such that $|T(f)| = 1/\sqrt{S(f)}$ will *whiten* the data. Fig. 1 also shows the PSD of the output of such a digital filter. In *RIDGE*, the whitening filters are Finite Impulse Response (FIR) filters and the filter coefficients are obtained using the PSD obtained from a user-specified training data segment. The digital filter is then applied to a longer stretch of data. It is clear that any non-stationarity in the noise floor on timescales shorter than the gap between the training and the processed data can create a discrepancy in the trained filter and the filter that is required for whitening the longer stretch. To the knowledge of the authors, not much concrete work exists in the GW literature on handling this issue robustly in any analysis pipeline. However, tools already exist that can monitor the behaviour of the noise floor in real time [7], and characterize burst-like non-stationary components [8]. We intend to integrate these information into our pipeline in the future.

The whitening step above is followed by a line estimation and removal step which reduces or, in some cases, eliminates the effect of strong narrowband noise features (*line* noise) arising from power line interference or violin modes. The method used here, called *MBLT*, is described in [6]. Essentially, the method consists of estimating the amplitude and phase modulation of a line feature at a given carrier frequency (which have to be found manually). Fig. 2 shows spectrograms of the whitened data before and after line removal. In this example, signals were injected into the data prior to line removal. As can be seen, the line removal does not affect the signals in

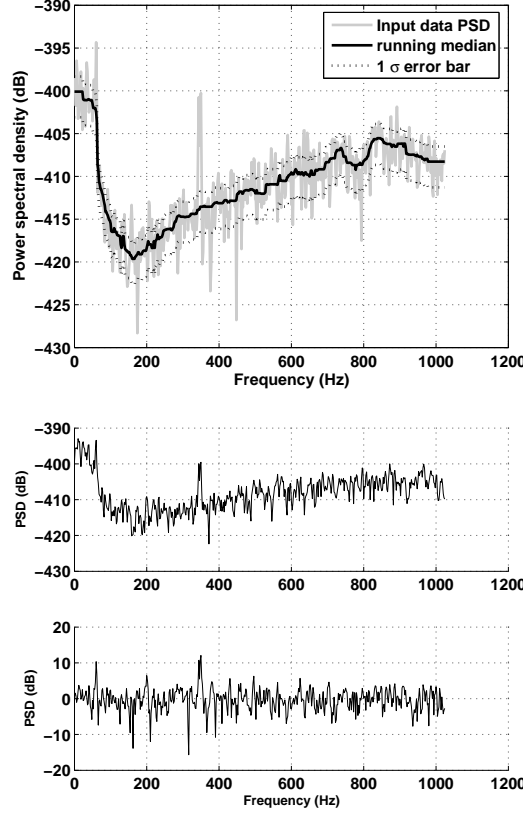


Figure 1. A sample power spectral density and the corresponding running median estimate of the noise (top plot). Note that the noise floor estimation was not affected by the large outlier due to a strong sinusoidal signal. The plot at the bottom shows the psd of raw data (top) and the psd (bottom) of the data after passing it through the whitening filter. The whitened data has variance 1, which explains the change in level to 0 dB in the bottom plot.

any significant way. This is an inbuilt feature of MBLT which uses the running median for estimation of the line amplitude and phase functions. Transients signals appear as outliers in the amplitude/phase time series and are rejected by the running median estimate. The whitened and line removed data is then passed on to the next step of RIDGE.

2.2. Detection statistic

The basic algorithm implemented for coherent network analysis in RIDGE is *regularized* maximum likelihood, described in several recent papers [9, 10, 11]. The GW response of any one detector is a linear combination of the two unknown polarization waveforms $h_+(t)$ and $h_\times(t)$ arriving at the detector from a certain direction θ_0, ϕ_0 on the sky. We assume the Earth-centered, ecliptic reference frame here for defining the polar angle, θ , and azimuthal angle, ϕ . It was shown in [9] that the problem of inverting a set of detector responses to obtain $h_+(t)$ and $h_\times(t)$ is an *ill-posed* one and needs to be

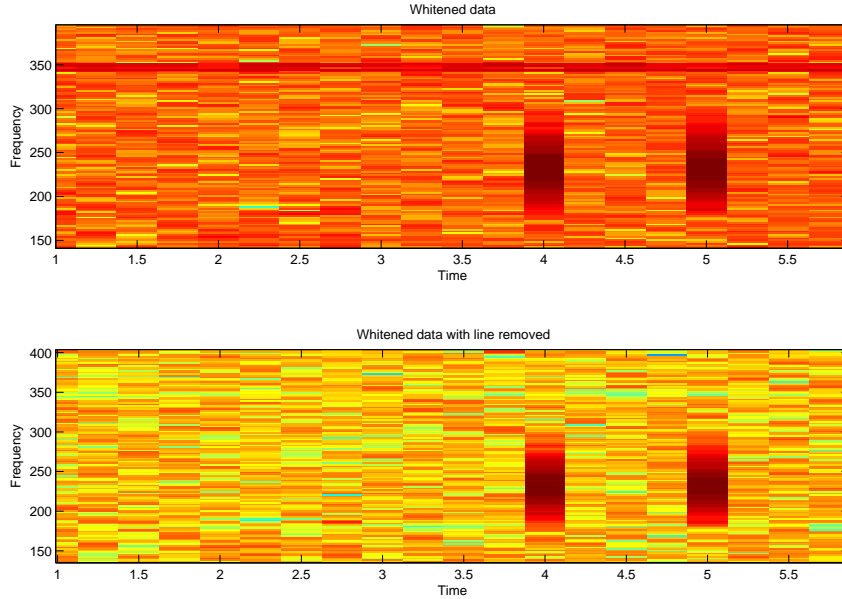


Figure 2. Spectrograms of simulated data with (top) line present in the data along with two transient signals and (bottom) same data with the line removed using MBLT. This simulation actually consisted of more lines but due to the limitations of the graphics used, we show only a zoomed in view of a particular region of the time-frequency plane. The simulated line feature appears as the straight horizontal line in the upper plot near 350 Hz; the feature actually consists of two closely spaced sinusoids at 344 and 349 Hz.

solved by using some kind of regularization. Alternatives to the regularization used in [9] were proposed in [10, 11]. The theoretical aspects of regularization related to the direction dependent antenna patterns of the detectors in a network is fairly well understood now.

The particular regularization scheme used to obtain the results reported here was developed in [10]. It is quite easily shown that the *hard constraint* algorithm presented in [9] is actually obtained in the limit of an infinitely large gain factor for the regulator of [10]. The input to the algorithm is a set of equal length, conditioned data segments from the detectors in a given network. The output, for a given sky location θ and ϕ , is the value of the likelihood of the data maximized over all possible h_+ and h_\times waveforms with durations less than or equal to the data segments. The maximum likelihood values are obtained as a function of θ and ϕ – this two dimensional output, $\mathbf{S}(\theta, \phi)$, is called a *sky-map*.

Fig. 3 shows examples of sky-maps obtained for the network consisting of the two 4km LIGO interferometers and the 2km LIGO interferometer. As can be seen from the figure, the presence of a signal can “ring off” the entire sky. As the direction to a trigger will usually be well known in advance from electromagnetic observations, say, there is no necessity in a triggered search to restrict ourselves only to a part of the sky-map for the purpose of detection. We can construct a detection statistic using the entire sky map. In the present paper, we consider two different choices. The obvious

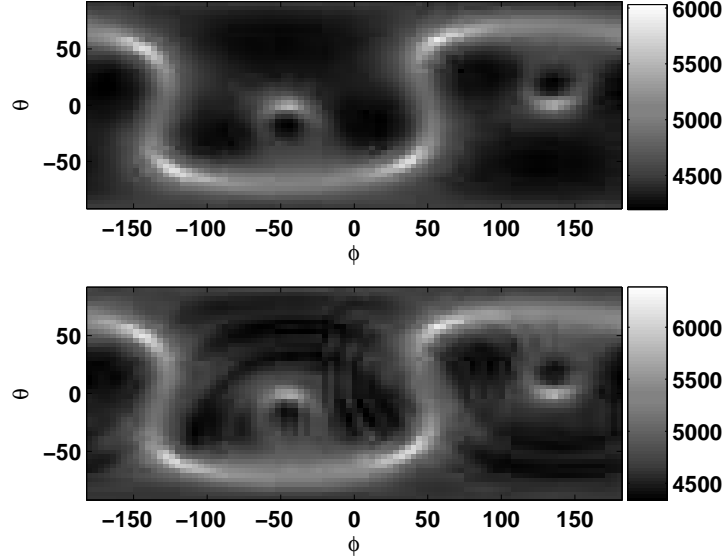


Figure 3. Plots of the sky-map for noise only case (top) and signal plus noise case (bottom). The detector network used was H1, H2, L1 and V1. The top plot was made by averaging the sky-maps for 100 noise realizations. The bottom plot is an average over sky-maps made with 4 independent realizations of noise plus a signal with $h_{\text{rss}} = 5 \times 10^{-22} \text{ Hz}^{-1/2}$ (c.f., Eq. 4). The magnitude scale is in arbitrary units. The test statistics are constructed by normalizing the maps.

one is (1),

$$R_{mm} = \frac{\max_{\theta, \phi} \mathbf{S}(\theta, \phi)}{\min_{\theta, \phi} \mathbf{S}(\theta, \phi)}. \quad (1)$$

$[\max / \min]_{\theta, \phi} \mathbf{S}(\theta, \phi)$ represents a [maximum/minimum] value of $\mathbf{S}(\theta, \phi)$ on the θ - ϕ plane. A less obvious choice is (2),

$$R_{\text{rad}} = \left[\left(\frac{\max_{\theta, \phi} \mathbf{S}(\theta, \phi)}{\max_{\theta, \phi} \bar{\mathbf{S}}_0(\theta, \phi)} - 1 \right)^2 + \left(R_{mm} \frac{\min_{\theta, \phi} \bar{\mathbf{S}}_0(\theta, \phi)}{\max_{\theta, \phi} \bar{\mathbf{S}}_0(\theta, \phi)} - 1 \right)^2 \right]^{1/2}, \quad (2)$$

$$\bar{\mathbf{S}}_0(\theta, \phi) = \text{E} [\mathbf{S}(\theta, \phi) | \text{no signal in data}], \quad (3)$$

where $\text{E}[\mathbf{S}(\theta, \phi) | \text{no signal in data}]$ denotes an ensemble average taken over realizations of sky-maps that do not have any GW signals. The second statistic, R_{rad} , is the radial distance of the observed values, in an appropriately scaled $(R_{mm}, \max_{\theta, \phi} \mathbf{S}(\theta, \phi))$ plane, from the mean location of the same quantities in the absence of a signal.

3. Results

We carried out Monte Carlo simulations to characterize the performance of the detection statistics R_{mm} and R_{rad} . The network consisted of the 4km LIGO detectors

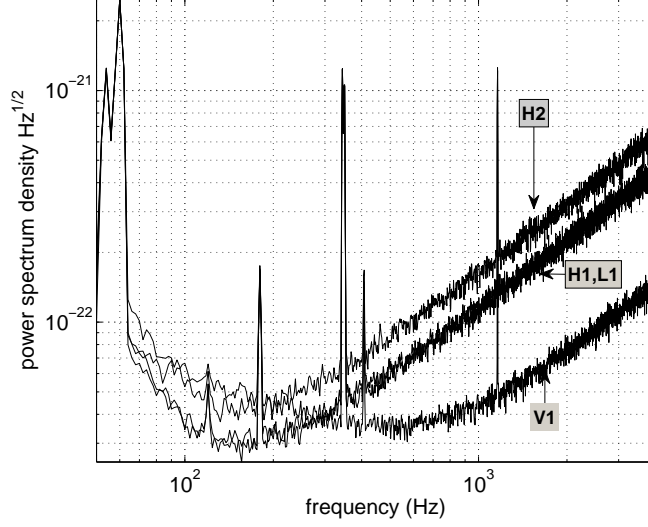


Figure 4. Power Spectral Densities of simulated detector noise for H1 (L1), H2 and V1. The power spectral densities were computed with a frequency resolution of 2.0 Hz.

(H1 and L1), the 2km LIGO detector (H2) and the Virgo detector (V1). For the detector noise PSD, we used the design sensitivity curves for the LIGO and Virgo detectors as given in [12, 13] and kept the locations and orientations the same as the real detectors. Gaussian, stationary noise was generated (~ 3000 sec) by first generating 4 independent realizations of white noise and then passing them through FIR filters having transfer functions that *approximately* match the design curves. To simulate instrumental artifacts, we added sinusoids with large amplitudes at (54, 60, 120, 180, 344, 349, 407) Hz. The resulting PSDs of the simulated data are shown in Fig. 4.

Signals of constant amplitude were added to the simulated noise at regular intervals. The injected signals corresponded to a single source located at $\theta = -30^\circ$ and $\phi = 167.0^\circ$, which was the location of a real trigger, GRB060813. We assumed that the $h_+(t)$ and $h_\times(t)$ waveforms were both sine-Gaussian signals having center frequency 235 Hz and a $Q = 9$. The $h_\times(t)$ waveform has an added phase of $\pi/2$ relative to the phase of $h_+(t)$. Fig. 5 shows the signals, i.e., the detector responses, that were added to the noise. The signal strength is specified in terms of the h_{rss} value, defined as

$$h_{\text{rss}} = \left[\int_{-\infty}^{\infty} dt (h_+^2(t) + h_\times^2(t)) \right]^{1/2}. \quad (4)$$

In our results we use h_{rss} values of 3×10^{-22} , 5×10^{-22} and $7 \times 10^{-22} \text{ Hz}^{-1/2}$.

The simulated data were generated at a sampling frequency of 16384 Hz and then passed through the data conditioning pipeline. Besides downsampling the data by applying the same anti-aliasing filter to all data streams, the data conditioning pipeline applies time domain whitening filters that were trained, as described earlier, on the first two seconds of data for each detector (without any injected signals). The

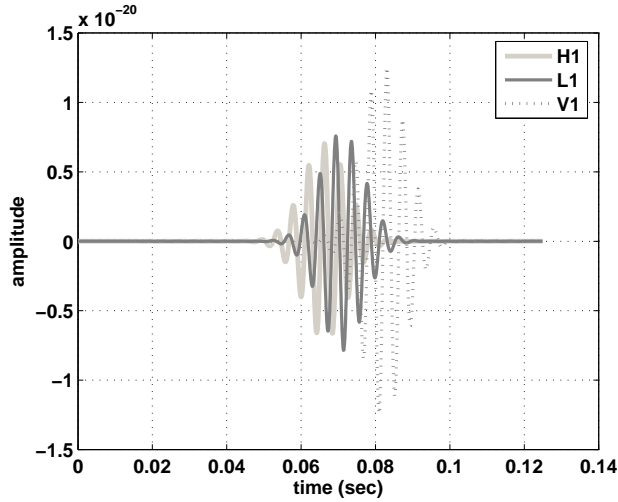


Figure 5. The detector responses to the injection signal used in the Monte Carlo simulations. The strain response for H1 and H2 are identical because of their co-location and co-alignment.

conditioned data is then passed to the sky-map generation code in segments of length 0.5 sec. This integration time is much larger than the ~ 40 msec duration of the injected signals and, hence, the performance estimates we obtain here should be taken as lower bounds. The reason behind the large choice of 0.5 sec was to accommodate the filter delays introduced into the data. In a future version of the pipeline, these delays, which are known since the filters are all FIR filters, will be removed carefully. This will allow us to shrink the integration time for short duration signals.

Fig. 6 shows the Receiver Operating Characteristic (ROC) curve for the simulation described above. ROC curves for both R_{mm} and R_{rad} are shown. Clearly, the R_{rad} statistics performs better than the more naive choice R_{mm} , demonstrating that a judicious choice of a statistic that incorporates information from the full sky-map is definitely required for triggered searches. We believe that more effective full sky-map statistics can be derived that can push performance to even better levels. For the current simulation and choice of parameters, we find that an h_{rss} of $5 \times 10^{-22} \text{ Hz}^{-1/2}$ can be detected with $\simeq 62\%$ probability at a false alarm probability of 10^{-2} . The false alarm probability corresponds to a rate of 1 false event in 50 sec.

4. Conclusion

We describe here an analysis pipeline, **RIDGE**, that implements regularized maximum likelihood based network analysis for triggered searches. Monte Carlo simulations with simulated detector noise show that the pipeline is quite sensitive: For a LIGO-Virgo network, a $\simeq 62\%$ detection probability is obtained for a signal $h_{rss} = 5 \times 10^{-22} \text{ Hz}^{-1/2}$ at a false alarm rate of $2 \times 10^{-2} \text{ Hz}$. All the algorithms used in this pipeline are significantly different from other network analysis pipelines [14, 15] that are also currently being applied to triggered searches. (The basic statistic used in [15] is the hard constraint statistic introduced in [9].) Thus, at both the level of algorithms

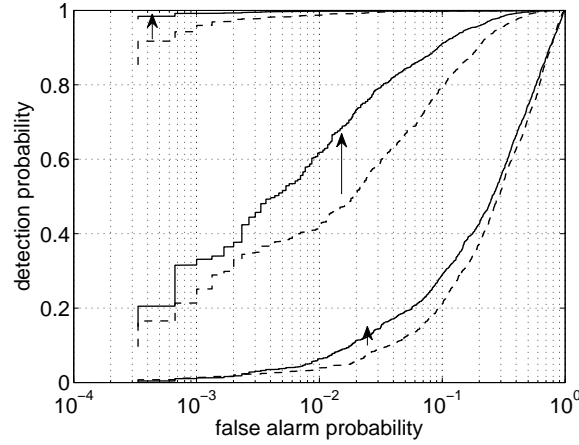


Figure 6. Receiver Operating Characteristics for R_{mm} (dashed) and R_{rad} (solid) for $h_{rss} = 3 \times 10^{-22}$ (bottom), 5×10^{-22} (middle) and $7 \times 10^{-22} \text{ Hz}^{-1/2}$ (top). The enhancement when going from R_{mm} to R_{rad} is shown by the arrows.

and the associated software, **RIDGE** should provide an independent check for results obtained with other pipelines. **RIDGE** is also being designed to serve as a platform for trying out new regulators. In future work, since **RIDGE** pipeline does not only extract candidates of gravitational wave signals, but also reconstruct h_+ and h_\times waveform at arbitrary sky location, we integrate a waveform estimation method [16] and investigate how accurately astrophysical information can be obtained.

Acknowledgments

K.H. is supported by NASA grant NAG5-13396 to the Center for Gravitational Wave Astronomy at the University of Texas at Brownsville. SDM's work was supported by NSF grant PHY-0555842. The work of S.D. and M.R. were supported by the Center for Gravitational Wave Physics at the Pennsylvania State University and the US National Science Foundation under grants PHY 00-99559, PHY 02-44902, PHY 03-26281, and PHY 06-00953. The Center for Gravitational Wave Physics is funded by the National Science Foundation under cooperative agreement PHY 01-14375. This paper has been assigned LIGO Document Number LIGO-P070045-01.

References

- [1] S D Mohanty, S Marka, R Rahkola, S Mukherjee, I Leonor, R Frey, J Cannizzo and J Camp, 2004, *Class. Quantum Grav.* 21 No 5 S765-S774
- [2] Global Coordinates Network, <http://gc.n.gsf.nasa.gov>
- [3] The LIGO Scientific Collaboration, 2007, LIGO-P040055-01-Z
- [4] Mereghetti, S., et al., 2005, *A & A*, 433-2, L9-L12
- [5] R. J. Dupuis, G. Woan, 2005, *Phys.Rev. D* 72 102002
- [6] S D Mohanty, 2002 *Class. Quantum Grav.* 19 No 7 1513-1519
- [7] S Mukherjee, 2003 *Class. Quantum Grav.* 20 No 17 S925-S936
- [8] K. Hayama and M.-K. Fujimoto 2006 *Class. Quantum Grav.* 23 S9-S15
- [9] S. Klimenko, S. Mohanty, M. Rakhmanov, G. Mitselmakher 2005 *Phys.Rev. D* 72 122002
- [10] M. Rakhmanov 2006 *Class.Quant.Grav.* 23 S673-S686

- [11] S. D. Mohanty, M. Rakhmanov, S. Klimenko, G. Mitselmakher 2006 *Class.Quant.Grav.* 23 4799-4810
- [12] http://www.ligo.caltech.edu/~jzweizig/distribution/LSC_Data
- [13] <http://www.virgo.infn.it>
- [14] S. Klimenko 2006 G060565-00-Z
- [15] S. Chatterji, A. Lazzarini, L. Stein, and P. J. Sutton, A. Searle, and M. Tinto, 2006, *Phys. Rev. D* 74, 082005, P J. Sutton and M Was, 2007 LIGO-T070091-00-Z
- [16] K. Hayama 2004 *Progress of Theoretical Physics* 111 vol.6 807